Effect of BPHA contamination on ^{68}Ga labelling to DOTA

Brenda Giling

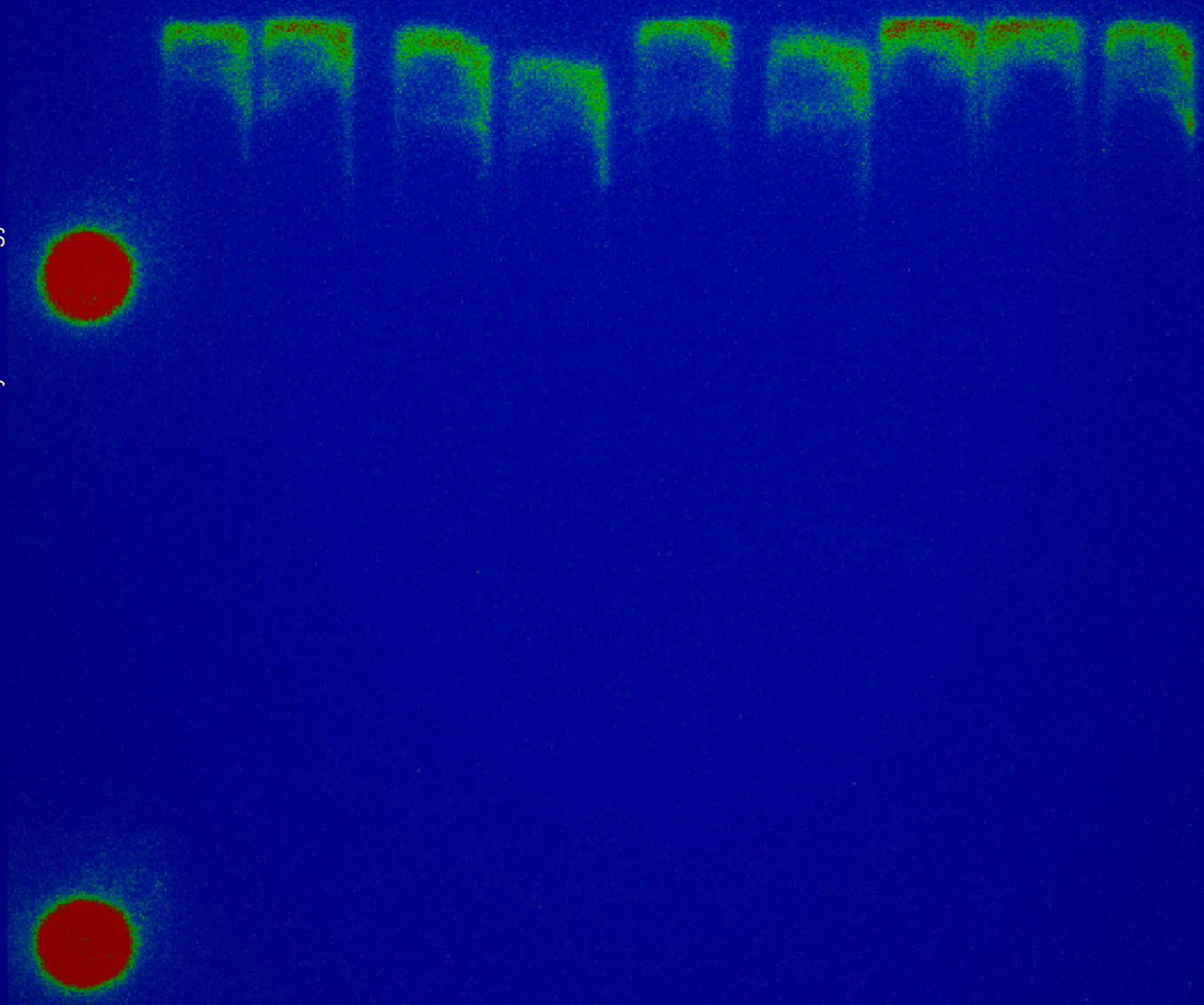

Delft University of Technology

TU Delft

Effect of BPHA contamination on ^{68}Ga labelling to DOTA

by

Brenda Giling

To obtain the degree of Bachelor of Science
at the Delft University of Technology,
to be defended on Monday August 1, 2022 at 1:00PM

Thesis supervisor:	Dr. ir. R. de Kruijff
Second examiner:	Dr. K. Djanashvili
Daily supervisor:	S. Trapp MSc
Project Duration:	April 2022 - August 2022
Institute:	Delft University of Technology
Faculty:	Applied Sciences
Department:	Reactor Institute Delft
Research group:	Applied Radiation Isotopes

TU Delft

Abstract

Towards 2040 the global cancer burden could rise to 28.4 million cases. Early diagnosis and treatment leads to a higher number of cancer survivors. ^{68}Ga is a promising radionuclide in radio-imaging, and it is often labelled with a labelling link called DOTA in radiopharmaceuticals. ^{68}Ga can be produced by a ^{68}Ge/^{68}Ga generator. However, the ^{68}Ge supply issue, disposal issue, and an increasing demand in radiotracers for radio-imaging have led to the development of cyclotron production. In this method ^{68}Ga nuclides are produced through proton irradiation of enriched ^{68}Zn solutions. The produced nuclides are extracted from the solutions using a chelator called BPHA. After back extraction, BPHA contamination remains in the final solution and could possibly interfere with the labelling of ^{68}Ga to DOTA. The two objectives of this research were to investigate the effects of BPHA contamination on the labelling of ^{68}Ga to DOTA, and whether the contamination could be washed from the extraction solution. Instant thin layer chromatography, a Wallac gamma counter, and phosphor imaging were used to determine the labelling efficiency in ^{68}Ga solutions with and without BPHA contamination. Experiments have shown that without BPHA contamination an average labelling efficiency of 102.3% $\pm$ 2.5% can be calculated from the phosphor imaging, crossing the 100% due to background correction, and an average labelling efficiency of 99.58% $\pm$ 0.07% can be calculated from the Wallac gamma counter. In solutions with BPHA contamination this labelling efficiency became 70.8670% $\pm$ 41.6798%, showing high error due to major differences in BPHA concentration per extraction solution. In an attempt to remove the BPHA contamination, the extraction solutions were washed with chloroform. The BPHA contamination was measured in UV-Vis absorption, and showed a decrease after one wash. The remaining absorption could be assigned to the solvent. This researched merely addressed the presence of contamination, and did not measure quantitatively. Further research could investigate the quantitative relationship between BPHA contamination concentration and the DOTA-labelling efficiency.

Contents

List of Figures

List of Tables

Nomenclature

Abbreviations

Abbreviation	Definition
BPHA	N-benzoyl-N-phenylhydroxylamine; CAS 304-88-1
Bq	Becquerel
C	Carbon
Cl	Chlorine
^{11}C-MET	L-[methyl-^{11}C]-methionine
cpm	Counts per minute
DOTA	2,2',2",2"'-(1,4,7,10-tetraazacyclododecane-1,4,7,10-tetrayl)tetraacetic acid; CAS 60239-18-1
DOTA-NOC	2-[[10-(4-aminobutyl)-7-(1-hydroxyethyl)-13-(1H-indol-3-ylmethyl)-16-(naphthalen-1-ylmethyl)-6,9,12,15,18-pentaoxo-19-[[3-phenyl-2-[[2-[4,7,10-tris(carboxymethyl)-1,4,7,10-tetrazacyclododec-1-yl]acetyl]amino]propanoyl]amino]-1,2-dithia-5,8,11,14,17-pentazacycloicosane-4-carbonyl]amino]-3-hydroxybutanoic acid
DOTA-TATE	(2S,3R)-2-[[(4R,7S,10S,13R,16S,19R)-10-(4-aminobutyl)-7-[(1R)-1-hydroxyethyl]-16-[(4-hydroxyphenyl)methyl]-13-(1H-indol-3-ylmethyl)-6,9,12,15,18-pentaoxo-19-[[(2R)-3-phenyl-2-[[2-[4,7,10-tris(carboxymethyl)-1,4,7,10-tetrazacyclododec-1-yl]acetyl]amino]propanoyl]amino]-1,2-dithia-5,8,11,14,17-pentazacycloicosane-4-carbonyl]amino]-3-hydroxybutanoic acid
DOTA-TOC	2-[4-[2-[[(2R)-1-[[(4R,7S,10S,13R,16S,19R)-10-(4-aminobutyl)-4-[[(2R,3R)-1,3-dihydroxybutan-2-yl]carbamoyl]-7-[(1R)-1-hydroxyethyl]-16-[(4-hydroxyphenyl)methyl]-13-(1H-indol-3-ylmethyl)-6,9,12,15,18-pentaoxo-1,2-dithia-5,8,11,14,17-pentazacycloicos-19-yl]amino]-1-oxo-3-phenylpropan-2-yl]amino]-2-oxoethyl]-7,10-bis(carboxymethyl)-1,4,7,10-tetrazacyclododec-1-yl]acetic acid; CAS 204318-14-9
cpm	Counts per minute
EC	Electron capture
F	Fluor
^{18}F-FDG	2-[^{18}F]fluoro-desoxy-D-glucose
Ga	Gallium
Ge	Germanium
H	Hydrogen
iTLC	Instant thin layer chromatography
LLE	Liquid-liquid extraction
N	Nitrogen
Na(Tl)	Sodium iodide doped with thallium
NET	Neuroendocrine tumor

Abbreviation	Definition
O	Oxygen
PET	Positron emission tomography
PI	Phosphor imaging
PMT	Photomultiplier tube
SG	Silica gel
TLC	Thin layer chromatography
UV-Vis	Ultraviolet and visible light
Zn	Zinc

Symbols

Symbol	Definition	Unit
A	Activity	Bq
cpm	Counts per minute	min^{-1}
I	Intensity	a.u.

1

Introduction

A worldwide estimation in 2020 showed 19.3 million new cancer cases and 10 million cancer deaths, with breast cancer at 11.7% of all cases, and lung cancer as leading cause of cancer deaths with 18% [59]. In The Netherlands, the total number of deaths due to cancer was 45,144 in 2019. This formed almost 30% of all deaths [11]. Towards 2040 the global cancer burden could rise to 28.4 million cases. Early diagnosis and treatment leads to a higher number of cancer survivors.

Visualizing the location and size of the tumor are crucial factors in cancer treatment. A way of doing so is through positron emission tomography (PET). PET scanning is also a method to inspect whether the cancer has spread and whether selected cancer therapies are effective [2, 14, 66]. In this imaging method a positron emitting radionuclide is brought to the tumor cell. The emitted positron travels a short distance, typically 1-2 mm [63], before interacting with an electron. This interaction causes annihilation of both the positron and electron, which in its turn causes the emission of two high-energy photons, both 511 keV, that travel into opposite directions [12]. Detectors surrounding the patient are hit by the two photons almost simultaneously. Tracing the photons' emission paths back to their original emission in image reconstruction gives the location of the positron emitter and therefore the location of the tumor cell [57, 51]. For optimal PET imaging, the radionuclide should be brought as close as possible to the tumor cell.

Tumor cells differ among other things from healthy tissue by their proteins on the surface of the cell, called the target proteins. Radionuclides can be labelled to a targeting molecule, resulting in so-called radiotracers, that specifically bind to these target proteins. When a patient is injected with a labelled radioactive isotope it accumulates around the tumor cells only. This type of therapy is called targeted radionuclide therapy, a schematic overview can be found in Figure 1.1. By bringing the radiation close to the tumor cells, damage to the healthy tissue is minimized and accurate images of the tumor can be made [19]. The choice of radioactive nuclide should consider half-life, decay energy and imaging opportunities.

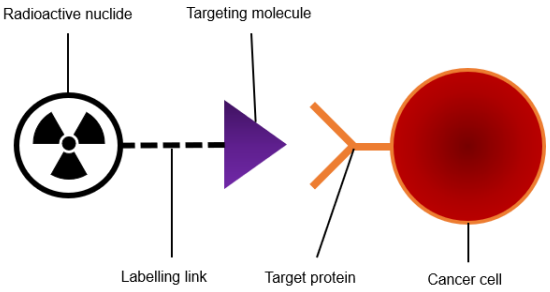

Figure 1.1: Schematic overview of targeted therapy. A targeting molecule with affinity for certain target proteins on tumor cells is linked to a radioactive nuclide. The tumor can be accurately visualized as the radioactive nuclide decays.

Radio-metals like ^{68}Ga have been investigated for their decay characteristics and targeting ability in radio-chemistry [65]. A simplified decay scheme of ^{68}Ga is shown in Figure 1.2 [68]. With a high positron emission fraction and a half-life of only 68 minutes, ^{68}Ga provides enough energy for PET imaging with fast blood clearance and target localization [64].

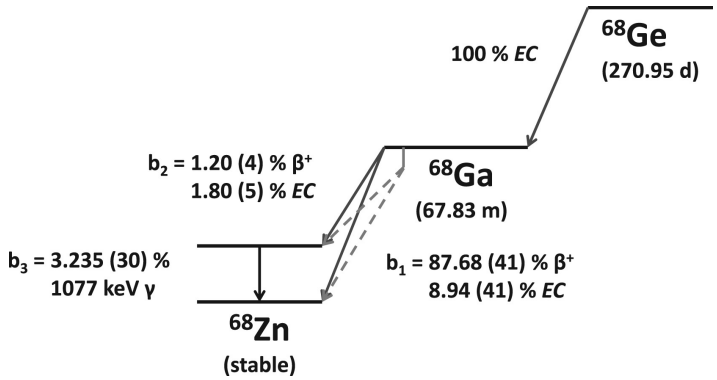

Figure 1.2: Decay scheme of ^{68}Ge to ^{68}Zn, main decay type is positron emission [68]

^{68}Ga can be produced in two ways, either by a ^{68}Ge/^{68}Ga generator or through proton irradiation of enriched ^{68}Zn solutions. The generator is commercially available and at low cost, but comes with considerable waiting times between elutions, as well as decreasing activity with time as the parent nuclide ^{68}Ge decays [6, 47]. With the increasing need for radiopharmaceuticals, the production method through ^{68}Zn solutions is an inexpensive way to obtain clinical radionuclides and its separation process for ^{68}Ga is researched to meet the demand. Enriched ^{68}Zn in nitric acid solutions are called liquid targets, and their irradiation is done in a cyclotron, a charged-particle accelerator [61, 38, 1]. This reaction is a ^{68}Zn(p,n)^{68}Ga reaction and the general equation for such (p,n) reaction is given in Equation 1.1 [12, 15]. Under irradiation of nucleus X, a high-velocity proton enters the nucleus while a neutron is lost, keeping the mass number A the same while increasing the proton number Z by one.

$$ {}^{A}_{Z}\mathrm{X} \rightarrow {}^{A}_{Z+1}\mathrm{X} \tag{1.1} $$

After irradiation of the ^{68}Zn target solution, the ^{68}Ga radionuclide needs to be separated from the liquid target. This can be done by liquid-liquid extraction combined with back-extraction. In liquid-liquid extraction, two immiscible solvents are brought together to create a two-phase system, usually one aqueous and one organic solvent. A chelator, a molecule that is able to bind metal ions, can be added to one of the solvents. This chelator selectively binds to the target compound, in this case the ^{68}Ga radionuclides, forming an hydrophobic complex. After shaking or vortexing, the radionuclide complexes move to the preferred solvent. When that extraction solvent loaded with the target compound is removed from the two-phase system, the target compound is successfully extracted from its original solution [37]. In so-called 'back extraction', the target compound is again extracted into a new extraction solvent. After

the back extraction process, the final ^{68}Ga solution is obtained.

In this research, production of ^{68}Ga through a ^{68}Zn target solution is imitated without cyclotron irradiation, and the organic phase in the liquid-liquid extraction consists of the N-benzoyl-N-phenylhydroxylamine (BPHA) [56] chelator in chloroform, with selectivity for ^{68}Ga. In the back extraction process, contamination of the BPHA and chloroform can end up in the final solution. Drying the final extraction solution removes the chloroform contamination, but BPHA contamination remains, as seen in the UV-Vis spectrum of Figure 1.3. The blue line represents absorption of the back-extraction, with high chloroform contamination. The black line shows BPHA contamination after drying and redissolving in water. The red line shows BPHA contamination after drying with addition of hydrogen peroxide and redissolved in water [62].

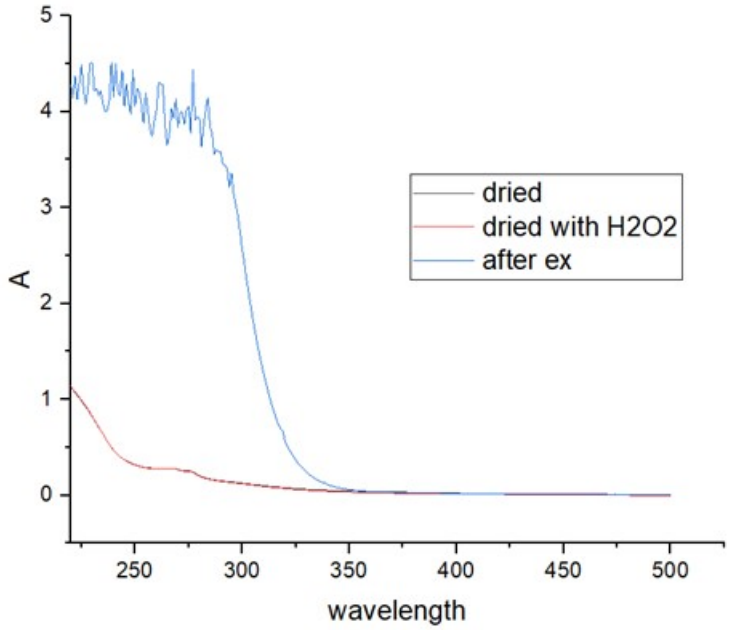

Figure 1.3: UV-Vis: BPHA contamination in the final back-extracted solution. Blue line shows absorption with high chloroform contamination. Black line shows BPHA contamination after drying and redissolving in water. Red line shows BPHA contamination after drying with addition of hydrogen peroxide and redissolved in water [62]

Remaining BPHA contamination after back extraction could potentially interfere with the labelling of the radionuclide to their targeting molecule in radiopharmaceuticals. To investigate the potential interference this research studies the labelling of ^{68}Ga with DOTA, a molecule often used as labelling link in radiopharmaceuticals [41]. Several targeting molecules can be bound to DOTA, such as DOTA-TOC, DOTA-TATE and DOTA-NOC, all with high affinity for somatostatin receptors [22, 30, 67]. These receptors are protein targets over-expressed in neuroendocrine tumors (NET), commonly found in the gastrointestinal tract (48%), lung (25%) and pancreas (9%) [43, 69]. DOTA and its targeting molecules creates stable chelates with various metal ions, resulting in radiotracers suitable for tumor imaging of NET [49, 25].
The fore-mentioned BPHA contamination could influence the DOTA labelling efficiency to ^{68}Ga as both chelators have affinity for the radionuclide. Decreased labelling efficiency would result in less radiotracers in the solution and negatively affecting the PET imaging efficiency.

In this report two research questions are answered:
1. Does BPHA contamination influence the labelling efficiency of ^{68}Ga radionuclides to the DOTA labelling link?
2. Can the BPHA contamination be removed from the final extraction solution, when ^{68}Ga is produced from enriched ^{68}Zn target solutions?

2

Background

In this chapter the background information for this research is presented. ^{68}Ga is discussed in its production methods, suitability as radiotracer and its labelling to the DOTA target molecule. The techniques used are discussed in section 2.2 and the equipment is presented in section 2.3.

2.1. ^{68}Ga-DOTA

A nuclide suitable for targeted radioimaging is ^{68}Ga, as discussed in the introduction. The positron emission percentage of 89% in decay would provide high quality imaging in PET [10]. Traditional radiotracers used in PET are [^{18}F]FDG, 2-[^{18}F]fluoro-desoxy-D-glucose, and [^{11}C]MET, L-[methyl-11C]-methionine, with half lives of 109.7 minutes and 20.39 minutes respectively [23, 58]. The very short half-life of ^{11}C limits the use of this nuclide in PET imaging. The facility needs an on-site cyclotron to produce the ^{11}C nuclides, as the nuclides decay too fast for long-distance transport [60]. [^{18}F]FGD was developed in radiotherapy to remove these practical issues, but it has a longer half-life and is not able to discriminate cancer from inflammation and infection [54, 42]. ^{68}Ga with a half-life of 68 minutes solves the transport-issues of ^{11}C and provides clear tumor imaging. The patient is exposed for shorter times and relieved from long treatment duration than with ^{18}F [64].

Production of ^{68}Ga can be done in two ways, either by a ^{68}Ge/^{68}Ge generator or through irradiation of enriched ^{68}Zn solutions. In a ^{68}Ge/^{68}Ga generator, the parent nuclide ^{68}Ge is adsorbed in an ion-exchange column, where it decays to its daughter nuclide ^{68}Ga. Four hours after elution ^{68}Ga radioactivity is regenerated and at least 60% of the ^{68}Ge-activity can be eluted as ^{68}Ga [27]. The yield decreases with time, as the parent nuclide decays with a half-life of 270.95 days [46, 47]. The ^{68}Ge/^{68}Ga generator is usually eluted with hydrochloric acid [29]. With short elution times of 2 minutes the generator is suitable for medical facilities without the need of an on-site cyclotron. However, the ^{68}Ge supply issue, disposal issue, and an increasing demand in radiotracers for PET imaging have led to the proposal of the second production method: cyclotron production [27].
As described in the introduction, cyclotron production of ^{68}Ga uses enriched ^{68}Zn target solutions. A cyclotron is a particle accelerator, which uses an electric field and magnetic field to give particles high velocity speeds and use them as projectiles in nuclear disintegration [31]. The magnetic field holds the particle in a horizontal plane. The electric current attracts the particle, and switches as the particle almost reaches the electric pole. By switching the electric current each time, the particle starts spiraling within the horizontal plane. As the high velocity is reached, the particle is set to collide with a nucleus. The impact of collision causes nuclear disintegration and changes the nucleus' structure [53, 13].
In cyclotron production of ^{68}Ga the target solution is bombarded by high-velocity protons, inducing the ^{68}Zn(p,n)^{68}Ga reaction [50, 38]. The ^{68}Ga radionuclides can be separated from the target solution by a technique called liquid-liquid extraction, also solvent extraction, which is discussed in detail in section 2.2.

Before radionuclides are ready to use in radiotherapy, they are linked to targeting molecules in a process called labelling, a schematic overview was given in the introduction Figure 1.1. The characteristic target

proteins on the surface of the tumor cell provide binding places for targeting molecules. When targeting molecules with specific chemical characteristics bind to the tumor, the labelled radionuclide, also called radiotracer, is brought close to the tumor cell.
Chelators are useful as labelling links between the radionuclide and targeting molecule, as they can bind metal ions to create a radiotracer stable enough for in vivo treatment [7]. In PET imaging of neuroendocrine tumors, targeting molecules bound to Dodecane Tetraacetic Acid (DOTA), 1,4,7,10-tetraazacyclododecane-1,4,7,10-tetraacetic acid, called DOTA-TOC, DOTA-TATE and DOTA-NOC, have promising affinity for the overexpressed somatostatin target proteins [44, 21]. Here, the DOTA serves as labelling link to the radionuclide, while the -TOC, -TATE and -NOC groups serve as targeting molecules. The carboxyl groups of DOTA can be fully protonated, this H_4DOTA structure is given in Figure 2.1 [41]. When ^{68}Ga is labelled to DOTA, chelation happens at the nitrogen and carboxyl groups and forms a kinetically and thermodynamically inert metal chelate [24]. To prevent activity loss, fast chelation is necessary for short-lived isotopes like ^{68}Ga [9]. When the radiotracer is unprotonated and ^{68}Ga is linked with the maximum coordinate number of six [8], the structure looks as shown in Figure 2.2 [26].

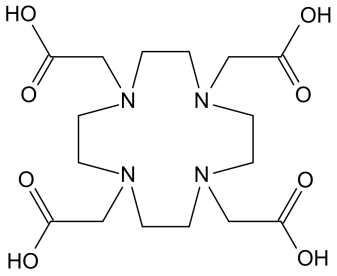

Figure 2.1: Molecular structure of the fully protonated chelating agent H_4DOTA [41]

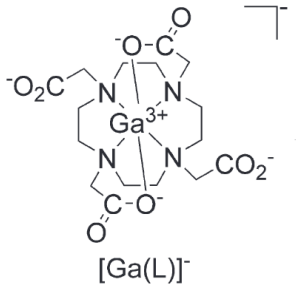

Figure 2.2: Depiction of the unprotonated ^{68}Ga-DOTA complex with a maximum coordination number of 6 [26].

2.2. Techniques

2.2.1. Liquid-liquid extraction / solvent extraction with back extraction

In liquid-liquid extraction (LLE), also called solvent extraction, the desired compound is separated based on its solubility in different solvents. LLE is a time and cost-effective separation technique and shows high recovery even with trace amounts of metals [34, 35]. The method combines two immiscible solvents, usually one aqueous and one organic, to create a two-phase system. A general overview of LLE is given in Figure 2.3. Liquid A is the original phase containing the desired compound. Liquid B, also called the extraction solvent, is added to liquid A (1) and the desired compound should have a higher solubility in B than in A. The system is shaken or vortexed to ensure good contact between the phases. Solvent B is now loaded with the desired compound and can be separated from the system (2) [28].
When a desired compound is insoluble in both phases, but extraction is necessary, an hydrophobic chelator can be added to the organic phase to form metal complexes with the desired compound. This causes the desired compound to reside in the organic phase.
LLE can be combined with back-extraction, also depicted in Figure **??**LLE$_{w}ith_{b}ack_{e}xtractionfigLLE_{w}ith_{b}ack_{e}xtractione$
$layersystem(3).Thesystemisshakenorvortexedtoensureadequatecontactbetween BandC.SolventCbecomesloadedwitht$
$extractionisatechniqueusedtoremovedesiredcompoundsfromaliquidorganicsolvent, anditprovidesfurtherpurification$

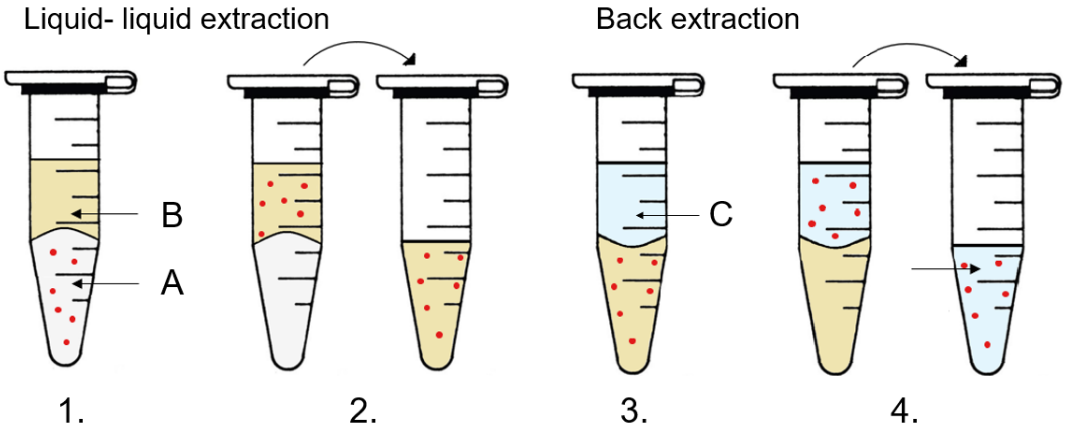

Figure 2.3: Overview of the liquid-liquid extraction process combined with back extraction. (1) Liquid A is the original phase loaded with desired compound; liquid B is added to create a two-phase system. (2) The system is shaken or vortexed and liquid B is now loaded with the desired compound; Liquid B is separated from the system. (3) Liquid C is added to the new system with loaded liquid B. (4) The system is shaken or vortexed and liquid C is now loaded with the desired compound; Separation of C further purifies the desired compound.

Liquid-liquid extraction combined with back extraction can be used after the production of ^{68}Ga in a cyclotron. Here, solution A in Figure 2.3 is the enriched ^{68} Zn in nitric acid target solution after irradiation, loaded with desired ^{68}Ga nuclides [38]. A suitable organic extraction phase for ^{68}Ga is the chelator N-benzoyl-N-phenylhydroxylamine (BPHA) [32] in chloroform. Chloroform was determined to be the most effective solvent for BPHA [52]. BPHA in chloroform forms the organic extraction solution B from Figure 2.3. The structures of BPHA and chloroform are depicted in Figure 2.4 and 2.5 respectively [56, 40]. BPHA forms hydrophobic complexes with the ^{68}Ga from the target solution, extracting the nuclides from the aqueous phase to the organic phase. Back extraction can be done with a low pH HCl solution, which protonates the BPHA and extracts the ^{68}Ga nuclides into the aqueous phase.

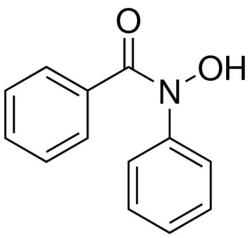

Figure 2.4: Structure of BPHA [56].

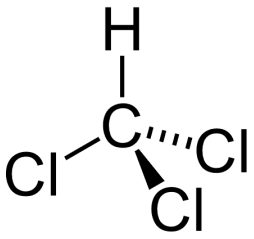

Figure 2.5: Structure of chloroform [55].

2.2.2. Instant thin layer chromotography (iTLC)

Thin layer chromatography (TLC) is used to separate compounds from a mixture based on their affinity for a mobile or stationary phase [5]. For instant thin layer chromatography (iTLC) the stationary phase is a binderless, glass microfiber chromatography paper impregnated with a silica gel (SG) [3], which can be conventionally cut with scissors and has faster developing time than traditional TLC. Depending on the affinity of a compound to the mobile phase, it is carried upwards on the strip. Acetonitrile 5% v/v can be used for the mobile phase, its structure depicted in Figure 2.6 [17].

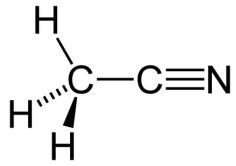

Figure 2.6: Molecular structure of acetonitrile [17].

The time that the iTLC strip stays in the mobile phase depends on the time it takes for the mobile layer to reach the top of the iTLC strip. Figure 2.7 provides an overview of the iTLC process in three steps. The mixed compound solution is brought onto an iTLC strip (A). The strip is then placed in the mobile phase, such that the mobile phase is below the application place. The mobile phase starts to move upwards on the iTLC strip (B). When the mobile phase has reached the top, the compounds in the original solution have separated based on affinity for the mobile phase (C).

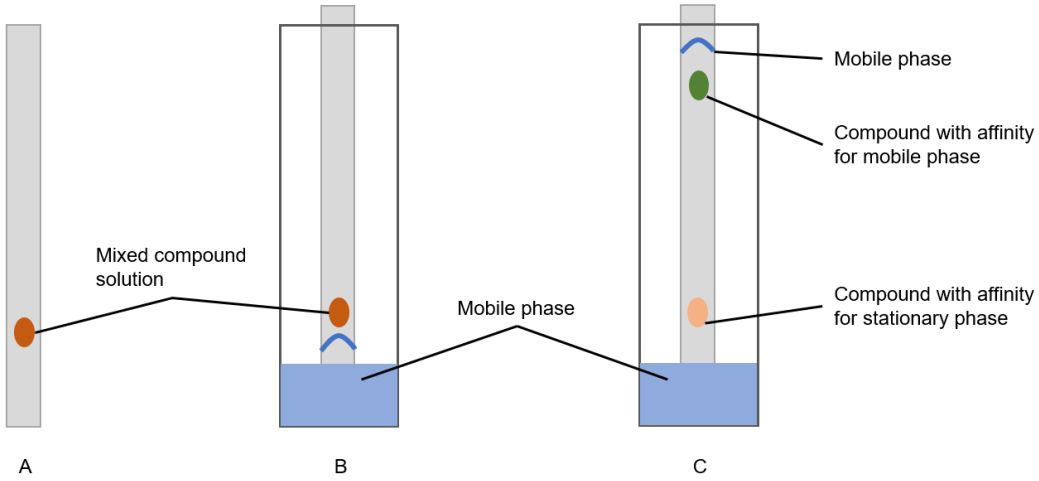

Figure 2.7: Overview of the iTLC process in three steps. (A) Application of the mixed compound; (B) Mobile phase moving upwards on the iTLC strip; (C) Separation of compounds based on affinity for the stationary or mobile phase.

In ^{68}Ga labelling to DOTA, the complex has affinity to the acetonitrile phase. Unlabelled ^{68}Ga nuclides have affinity for the stationary phase. When the iTLC strip is put into the mobile phase, the ^{68}Ga-DOTA complexes are carried upwards and the unlabelled ^{68}Ga nuclides stay behind. Using iTLC, the complexes can be separated from the ^{68}Ga nuclides.

2.2.3. Washing and drying

The characteristic solubility of a compound in different solvents can also be used to remove impurities from a solution. After the liquid-liquid extraction, BPHA contamination from liquid B in Figure 2.3 resides in the final aqueous extraction solution C. An organic solvent can be added to form a two-phase system and remove the impurity from solution C by a process called *washing*. The liquid-liquid extraction and washing processes are similar, but in washing the compound is unwanted and removed from the system, where in liquid-liquid extraction the compound is wanted and kept inside the system. Fresh chloroform is a good solvent for BPHA [52]. As BPHA is more soluble in chloroform than in HCl solution, adding chloroform to the system will move BPHA from the aqueous phase into the organic phase. Shaking or vortexing the system will ensure good contact between the two phases.The BPHA will reside in the organic phase as the aqueous phase is extracted, therefore 'washing' the contamination from the aqueous phase. Drying the solution will remove any traces of the chloroform, with a boiling point of 61.1 degrees Celcius [40]. After redissolving, any BPHA contamination left in the solution can be measured using UV-Vis, discussed in section 2.3.3.

2.3. Equipment

2.3.1. Phosphor imaging

In phosphor imaging (PI), radioactivity can be visualized and quantified. The technique uses so-called storage phosphors, which can store energy from X-rays or radioactivity [48]. When storage phosphors are exposed, they trap excited electrons from their valence band into their conduction band. This process is called the *first exposure*. The first exposure is done on a phosphor screen of storage phosphors, inside a light-tight casette so that only the radioactivity excites the storage phosphors. The phosphor

screen can be 'read' inside a phosphor imager. Here, the *second exposure* takes place, where low-frequency light on the storage phosphors causes the excited electrons to fall back from the conduction band to the valence band. This process is paired with emission of blue light, proportional to the excited electrons, which can be enhanced in a photomultiplier tube (PMT). In the phosphor imager, this creates a map of the excited electrons from the phosphor screen. Places on the phosphor screen with more excited electrons become more intense on the map, creating a visualization of the amount of radioactivity that was present on that part of the screen.
In an imaging toolbox program, selections on the map can be made to determine the intensity in that area. As discussed in section 2.2.2, in ^{68}Ga labelling to DOTA the ^{68}Ga-DOTA complex has affinity for the mobile phase and moves up on the strip. Unlabelled ^{68}Ga nuclides stay behind at the bottom of the strip. When the iTLC strip is used in the phosphor imaging process, the intensities at the top and bottom of the strip can be visualized and determined. The labelling efficacy of ^{68}Ga to DOTA can be calculated by taking these intensities and dividing the top value by the total intensity value, as given in Equation 2.1.

$$\text{Labelling efficiency} = \frac{I_{top}}{(I_{top} + I_{bottom})} * 100\% \tag{2.1}$$

2.3.2. Wallac gamma counter

In the Wallac gamma counter gamma rays of certain energy can be measured. During measurement time, the radiated gamma rays from the sample hit a NaI(Tl) scintillation crystal, exciting electrons from the ground state to an excited state. When these electrons fall back from the excited state, it is paired with the emission of a photon. The photon is multiplied in a photomultiplier tube (PMT) that is connected to the scintillation crystal on one end and has a detector on the other end. When the multiplied photons hit the detector, the amplitude of the output voltage is proportional to the amount of photons, and therefore proportional to the energy of sample's radiation [12]. The geometry of the samples should be the same to keep the comparison of results reliable. In this research, the Wallac is used for quantitative analysis of the iTLC strips to compare the separated compounds, namely unlabelled ^{68}Ga and DOTA labelled ^{68}Ga, and determine the DOTA labelling efficiency. Equation 2.2 can be used for the labelling efficiency, using the measured counts per minute (cpm) from the Wallac gamma counter.

$$\text{Labelling efficiency} = \frac{cpm_{top}}{(cpm_{top} + cpm_{bottom})} * 100\% \tag{2.2}$$

2.3.3. UV-Vis

UV-Vis spectroscopy takes place within the ultraviolet (UV) and visible light (Vis) spectrum, with wavelengths 10-400nm and 400-800nm respectively [4]. In a UV-Vis spectrophotometer a solution is exposed to light of certain wavelengths. A molecule present in the solution absorbs the light based on the wavelength. Measuring the absorption at different wavelengths creates an absorption spectrum [39] of this molecule. By comparing the measured absorption spectrum to characteristic absorption spectra in literature, the identity of the compound present in the solution can be determined. As the absorption of light increases with increasing concentration, UV-Vis can be used as a qualitative and quantitative analysis method, and the technique is able to detect small amounts of contamination in aqueous solutions [45]. In UV-Vis measurement a reference solution is used, usually the solvent, to account for any absorption not caused by the present molecule.

3

Materials and methods

In this section the used chemicals, instrumentation and process steps are discussed. This includes the extraction, labelling, iTLC, phosphor imaging and UV-Vis processes.

3.1. Chemicals

An overview of chemicals used is given in Table 3.1.

Table 3.1: Overview of chemicals used.

Used material	Product name	Supplier
iTLC paper	iTLC-SG	Agilent
MilliQ	Ultrapure water	Merck Milli-Q Advantage A10
5% Acetonitrile (v/v%)	Acetonitrile; CAS 75-05-08 Ultrapure water	Central warehouse L&M Merck Milli-Q Advantage A10
0.42mM DOTA	2,2',2",2"'-(1,4,7,10-tetraazacyclododecane-1,4,7,10-tetrayl) tetraacetic acid; CAS 60239-18-1 Ultrapure water	CheMatech
1 M Acetic acid buffer pH4.2	Acetic acid; CAS 64-19-7 Sodium acetate; CAS 127-09-3 Ultrapure water	Merck Sigma Merck Sigma Merck Milli-Q Advantage A10
HCl solutions	Hydrochloric acid; CAS 7647-01-0 Ultrapure water	VWR International B.V. Merck Milli-Q Advantage A10
BPHA in chloroform	N-Benzoyl-N-phenylhydroxylamine; CAS 304-88-1 Chloroform >99.8%; CAS 67-66-3	VWR International BV Central warehouse L&M
Target solution	Zinc nitrate hexahydrate 98%; CAS 10196-18-6 Nitric acid 65% REAG. ISO; CAS 7697-37-2	VWR International Central Warehouse L&M

3.2. Instrumentation

An overview of the lab instrumentation is given in Table 3.2.

Table 3.2: Overview of used instrumentation.

Used instrument	Product name	Manufacturer
Phosphor imager	Typhoon Trio+	Amersham GE
Scanning program	Typhoon Scanner Control v5.0	
Image Analysis Toolbox	ImageQuant TL	
Phosphor screen		
Screen eraser	Amersham Screen Eraser	
Exposure casette		
Thermoshaker	AccuTherm Microtube Shaking Incubator	Labnet
	Model I-4002-HCS	
Vortex	Vortex-Genie 2	Scientific Industries
pH meter	744 pH meter	Metrohm
Automatic Gamma Counter	Wallac Wizard 2480	PerkinElmer
Magnetic hotplate stirrer	VMS-A S040	VWR
Pipettes, ranges:		
1-5mL		Biohit
200-1000uL		Gilson
100-1000uL		Biohit
20-200uL		Gilson
2-20uL		Gilson
^{68}Ge/^{68}Ga generator		Eckert & Ziegler
Precision balance		Mettler-Toledo B.V.
UV-Vis spectrophotometer	UV-6300PC Double Beam	VWR
	Spectrophotometer	
	UV-Vis Analyst version 5.44 2014	
Cuvettes 1050uL	Quartz Absorption Cells	Purshee Experiment

3.3. Extraction from a $Zn(NO_3)_2$ target solution

A target solution of 300 uL 2M $Zn(NO_3)_2$ in 0.01 M HNO_3 was spiked with 10-30 kBq Ga^{68} that was eluted from the $^{68}Ge/^{68}Ga$ generator. This process was done in triplicate, giving batch 1-3, and the activity of the spiked target solutions was measured in the Wallac gamma counter. 300 uL of 200 mM BPHA in chloroform (>99.8%) was added to every batch and the solutions vortexed for 10 minutes at the highest speed. Then, 250 uL of the loaded organic phase was pipetted into a new Eppendorf. For the back-extraction, 250 uL of 2 M HCl was added to the loaded organic phase, keeping the ratio 1:1 between the organic and aqueous phase. The solution was vortexed at 10 minutes at highest speed. From the loaded aqueous phase, 200 uL was separated into a glass vial. The solution was dried down for 15 minutes at temperature '4' on the hotplate. The ^{68}Ga was redissolved in 3 mL 0.1 M HCl and measured in the Wallac spectrometer. By drying down chloroform contamination was removed, but the BPHA contamination remained. By drying and redissolving in 0.1 M HCl, the final extraction solution contained the same compounds as if the ^{68}Ga was eluted from the generator, the only difference being the BPHA contamination. The redissolved solutions were used in further DOTA labelling.

3.4. Labelling of DOTA to ^{68}Ga

To investigate the effect of BPHA on the DOTA labelling to ^{68}Ga, the labelling process was performed with ^{68}Ga solution eluted from the generator, as well as with ^{68}Ga solution from the extraction process. To three Eppendorfs was added: 120 uL acetic acid buffer pH4.2, 25 uL 0.42 mM DOTA in MilliQ and 25uL ^{68}Ga solution (10-30 kBq), either from the extraction process or eluted from the generator. The solutions were put in the thermoshaker for 15 minutes, at 90 degrees Celcius and 300 rpm. The ^{68}Ga-DOTA solutions were used in the iTLC process.

3.5. iTLC

For every labelling batch, three iTLC strips of 15 cm x 0.8 cm were prepared with 5 uL of DOTA-labelled or unlabelled ^{68}Ga solution, at 3 cm from the bottom of the strip. The strips were left to dry for 30 minutes, before putting them in acetonitril 5% v/v, submerging the strip 1 cm from the bottom. The mobile phase was left to run for 5 minutes, until it almost reached the top. The strips were left to dry for another 30 minutes. A 'test' strip was made by applying 2 uL of Ga^{68} from the $^{68}Ge/^{68}Ga$ generator 3 cm from the top and 3 cm from the bottom of the strip. This would later serve as reference point in the phosphor imaging.

3.6. Phosphor imaging

The iTLC strips were aligned in a plastic sleeve to prevent contamination of the machinery. The phosphor screen was erased in the eraser for at least 10 minutes. The screen was exposed to the iTLC strips for 10 minutes in a black box. The exposed screen was put immediately onto the phosphor imager. The option 'Best Resolution' was chosen and the pixel size set to 50 microns. The .GEL file was opened in Image Quant TL and the colours set to 'Pseudo colours I'. The top and bottom of each strip were selected and analyzed in the ImageQuant Toolbox, also measuring the background to determine labelling efficiency.

3.7. Wallac gamma counter

iTLC strips were cut 4 cm from the bottom and 4 cm from the top, and analyzed in the Wallac gamma counter. A ^{68}Ga protocol was used and measurement time was 2 minutes. The gamma counter efficiency was 0.0321 Bq/cpm. The DOTA labelling efficiency was determined for the eluted, DOTA-labelled ^{68}Ga solution, using Equation 2.2.

3.8. UV-Vis measurements

For the UV-Vis measurements 1050 uL cuvettes were used and analysed over 200-500 nm wavelength. A solution of 0.1 M HCl was used as reference to zero the equipment, as the measured solution was redissolved in 0.1 M HCl. Measurements were taken of the extraction solutions used in DOTA labelling and of the extraction solutions used in washing.

3.9. Washing extraction solutions

The back extraction process was done without ^{68}Ga-activity in triplicate, to create three BPHA contaminated extraction solutions. For every back extraction, 5 mL 200 mM BPHA in chloroform was added to 5 mL 2 M HCl. The solution was vortexed for 1 minute. 4.5 mL of 2 M HCl was separated into a drying vial. The solution was dried on the hotplate at temperature '4' to remove chloroform contamination. 4.5 mL of 0.1 M HCl was added to the drying vial for redissolving. From the 0.1 M HCl solution, 1050 uL was transferred to a cuvette to measure the BPHA starting contamination in UV-Vis. From the same 0.1 M HCl solution, 3 mL was transferred into a washing vial and 3 mL chloroform was added, keeping the ratio 1:1. The solution was vortexed for 1 minute. 2.5 mL of 0.1 M HCl solution was separated into a drying vial, and dried on the hotplate at temperature '4' to remove chloroform contamination. 2.5 mL of 0.1 M HCl was added for redissolving. From this solution 1050 uL was transferred to a cuvette and the BPHA contamination after one wash was measured in UV-Vis.

4

Results

In this chapter the results of the extraction process, labelling process and the UV-Vis measurements are presented. Pictures were made in the phosphor imager of the following ^{68}Ga solutions: extracted and unlabelled, eluted and DOTA-labelled, extracted and DOTA-labelled. The extraction solutions used in DOTA-labelling to ^{68}Ga were measured in UV-Vis for BPHA contamination. Results of the phosphor imager are presented in section 4.1. UV-Vis measurements of the extraction solutions used in labelling are presented in section 4.2.UV-Vis was also done in the washing process of contaminated extraction solutions and the graphs are included in section 4.3.

4.1. Phosphor imaging of different ^{68}Ga solutions

The phosphor imaging process was done for three different ^{68}Ga solutions: extracted and unlabelled (1), eluted and DOTA-labelled (2), and extracted and DOTA-labelled (3). Figure 4.1 provides an overview of four typical iTLC strips found in this research. In the figure, five iTLC strips are shown, namely:
Strip R) Reference iTLC, with eluted ^{68}Ga applied 3 cm from the bottom and 3 cm from the top.
Strip 1) Extracted ^{68}Ga, unlabelled.
Strip 2) Eluted ^{68}Ga, DOTA-labelled.
Strip 3A) Extracted ^{68}Ga, DOTA-labelled, high BPHA contamination.
Strip 3B) Extracted ^{68}Ga, DOTA-labelled, low BPHA contamination.

The iTLC from Figure 4.1 were taken from their original phosphor image to provide an overview. The complete phosphor images can be found in Appendix A. Three batches were made per ^{68}Ga solution, and were named batch 1, 2 and 3. For every batch, three iTLC strips were made, named A, B and C, totalling 9 iTLC strips per ^{68}Ga solution in the phosphor imager.

Using the ImageQuant TL Toolbox, areas were selected for the top and bottom of the iTLC in the phosphor image. In Figure 4.1, 4.2 and Appendix A these areas are indicated by the green borders. The areas were named ‘Bot’ for the bottom of the iTLC and ‘Top’ for the top of the iTLC. The reference iTLC strip was named ‘Test’. The intensity was measured in arbitrary units and corrected for the background intensity.

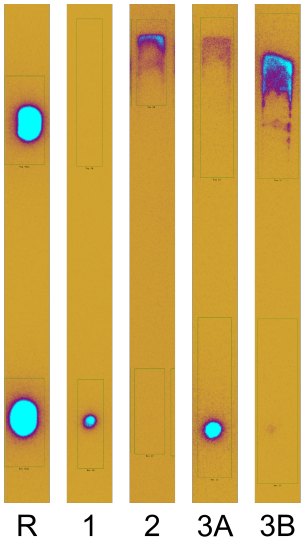

Figure 4.1: Overview of four typical iTLC strips under the phosphor imager. (R) Reference strip with eluted ^{68}Ga activity applied 3 cm from the bottom and 3 cm from the top. (1) iTLC strip of extracted, unlabelled ^{68}Ga solution. (2) iTLC strip of eluted ^{68}Ga solution labelled with DOTA. (3A, 3B) iTLC strips of extracted ^{68}Ga labelled with DOTA.

The labelling efficiency of DOTA to ^{68}Ga was calculated from the ImageQuant TL Toolbox using Equation 2.1 from subsection 2.3.1. The full raw data of the ImageQuant TL analysis is included in Appendix B.2. Strip 1A was seen to be influenced by its neighbouring reference strip. An example of this influence is given in Figure 4.2, taken from the phosphor image of extracted, DOTA-labelled ^{68}Ga in Appendix A. The average labelling efficiency was calculated per batch, and combined to form the average labelling efficiency for the ^{68}Ga solution. These values are given in Table 4.1.

Table 4.1: Labelling efficiencies using ImageQuant TL for the three different ^{68}Ga solutions given per batch and the total average labelling efficiency. The raw data is included in Appendix B.2

Type of ^{68}Ga solution	Batch 1	Batch 2	Batch 3	Average labelling efficiency
Extracted, unlabelled	1.499%	-0.08841%	-0.10291%	0.4358% $\pm$ 0.7516%
Eluted, DOTA-labelled	105.87%	100.254%	100.810%	102.3% $\pm$ 2.5%
Extracted, DOTA-labelled	11.93676%	101.438%	99.2265%	70.8670% $\pm$ 41.6798%

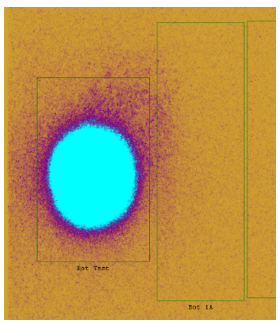

Figure 4.2: Example of the influence of the reference 'Bot Test' iTLC on its neighbouring 1A strip.

The activity on the top and bottom of iTLC strips 1A, 2A and 3A from eluted, DOTA-labelled ^{68}Ga solution was also measured in the Wallac gamma counter. The labelling efficiencies were calculated, the values are given in Table 4.2. The raw data can be found in Appendix B.1.

Table 4.2: Labelling efficiencies using the Wallac gamma counter for eluted, DOTA-labelled ^{68}Ga solution given per batch and the total average labelling efficiency. The raw data is included in Appendix B.1

Type of ^{68}Ga solution	Batch 1	Batch 2	Batch 3	Total average labelling efficiency
Eluted, DOTA-labelled	99.49%	99.59%	99.66%	99.58% +- 0.07%

4.2. UV-Vis of the extraction solutions from the phosphor imaging process

The extraction ^{68}Ga solutions used in the DOTA-labelling process were measured for their BPHA contamination in UV-Vis. The absorption spectrum is given in Figure 4.3, where the blue, red and green line represent the extraction solutions used in batch 1, 2 and 3 respectively.

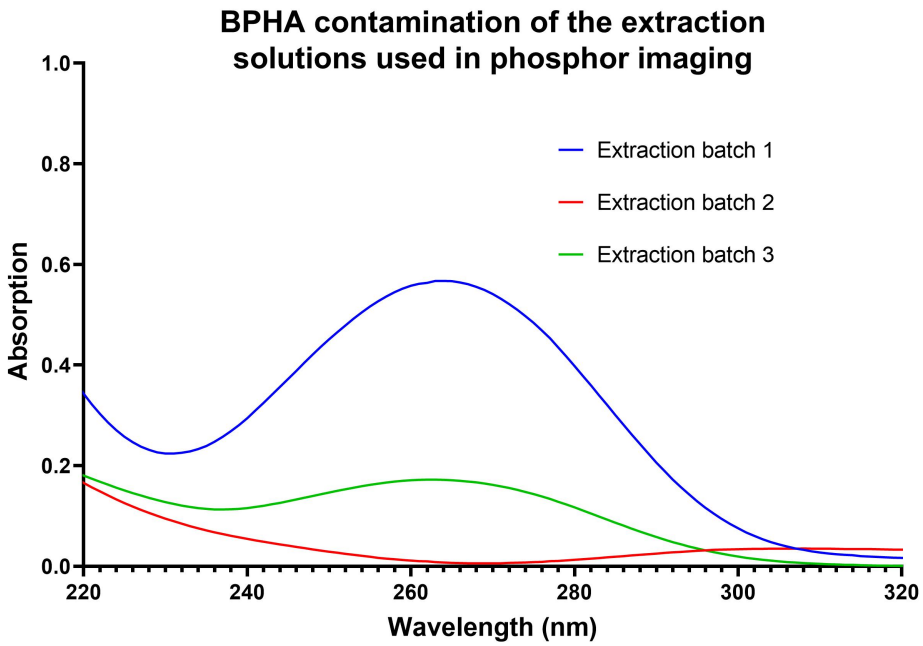

Figure 4.3: UV-Vis spectrum of the BPHA contamination of the three extraction solutions used in phosphor imaging of extracted, DOTA-labelled ^{68}Ga solution. The blue, red and green line represent the extraction solutions used in batch 1, 2 and 3 respectively.

4.3. UV-Vis of the washed extraction solutions

In an attempt to remove the BPHA contamination, back extraction solutions were washed with chloroform. Extraction was performed without ^{68}Ga-activity. The solutions after back extraction were measured before and after washing. Figure 4.4, 4.5 and 4.6 provide graphs of the UV-Vis measurements done on three extraction solutions. The reference was 0.1 M HCl. The blue line shows the UV-Vis absorbance before the washing process, and the red line shows absorbance after washing the extraction solution once.

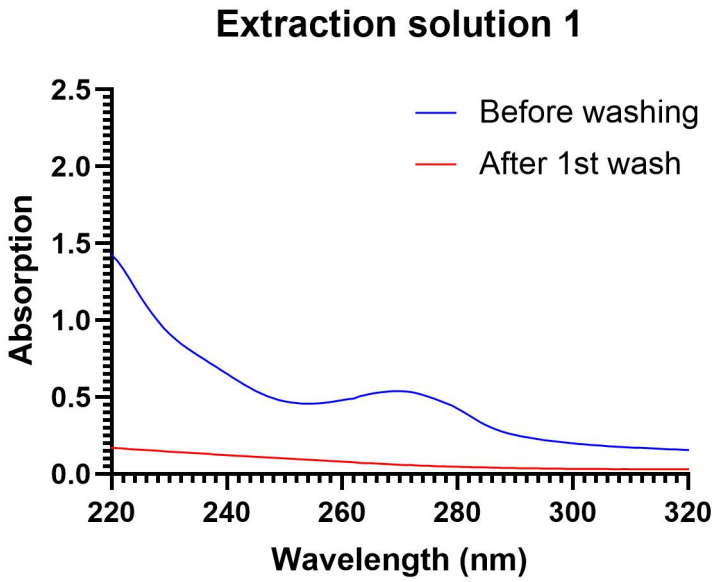

Figure 4.4: UV-Vis spectrum of extraction solution 1 before and after washing with chloroform. Reference 0.1M HCl.

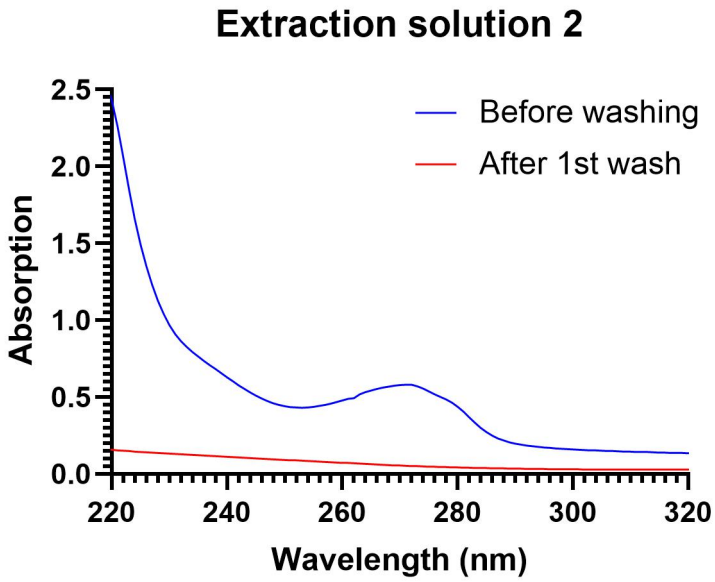

Figure 4.5: UV-Vis spectrum of extraction solution 2 before and after washing with chloroform. Reference 0.1M HCl.

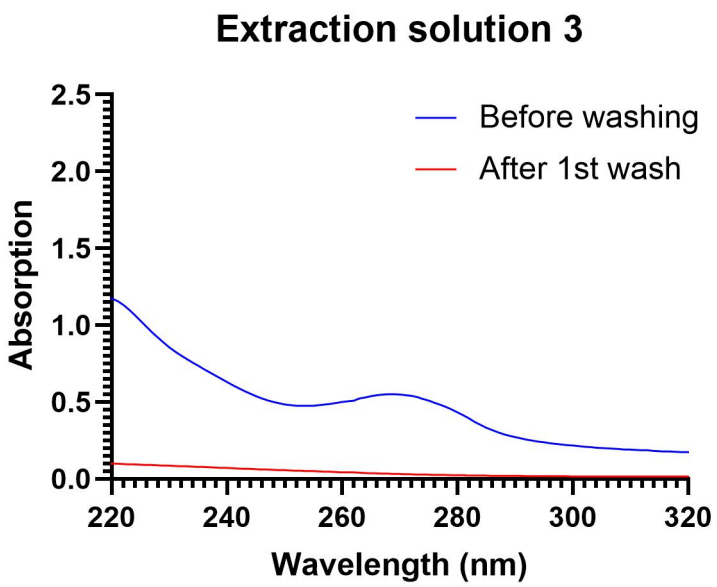

Figure 4.6: UV-Vis spectrum of extraction solution 3 before and after washing with chloroform. Reference 0.1M HCl.

5 Discussion

This chapter is separated into two sections. Section 5.1 discusses the main scope of this research, namely the influence of BPHA contamination on labelling ^{68}Ga to DOTA. In section 5.2 the UV-Vis measurements of section 4.3 are analyzed, where extraction solutions were washed with chloroform.

5.1. Influence of BPHA contamination on labelling of ^{68}Ga to DOTA

To determine the influence of BPHA contamination on the labelling of ^{68}Ga to DOTA, three different ^{68}Ga solutions were obtained: extracted and unlabelled (1), eluted and DOTA-labelled (2) and extracted and DOTA-labelled (3). The ^{68}Ga was extracted from Zn target solutions, imitated as if the solution was produced in a cyclotron. The organic phase contained BPHA which chelated the nuclides and moved the ^{68}Ga into the organic phase. Back extraction was done with HCl solution to protonate the BPHA and release the ^{68}Ga nuclides from the complex into the aqueous phase. After back extraction BPHA contamination in the final extraction solution occurred. The different solutions were used in iTLC and the strips were used in the phosphor imaging process. The labelling efficiency for the different solutions were calculated in the ImageQuant TL analysis on the phosphor images and the Wallac gamma counter.

Extracted and unlabelled ^{68}Ga solution contained BPHA contamination. The iTLC and phosphor imaging processes showed where the unlabelled nuclides end up on the iTLC strip in presence of BPHA contamination. From the phosphor images in Figure 4.1, strip (1), it can be seen that extracted and unlabelled ^{68}Ga has an affinity for the stationary phase, and ends up on the bottom of the strip. This reflects in a low average labelling efficiency of 0.4358% $\pm$ 0.7516%, calculated in the ImageQuant TL Analysis.

The eluted, DOTA-labelled ^{68}Ga showed affinity for the mobile phase, seen in Figure 4.1, strip (2). Successfully labelled nuclides showed up at the top of the iTLC strip. The solutions contained no BPHA contamination, and had an average labelling efficiency of 102.3% $\pm$ 2.5% in the ImageQant TL toolbox. Some intensities turned out negative after background correction, as can be seen from the raw data in Appendix B.2. For this reason, labelling efficiencies can reach negative percentage values or lie above 100%. In the Wallac gamma counter, average efficiency was calculated at 99.58% $\pm$ 0.07%. This shows that the labelling process conditions were ideal for DOTA-labelling to ^{68}Ga. The negative intensities could be assigned to the sensitivity of the phosphor plate. When transferring the plate from the exposure box to the phosphor imager, the plate was briefly exposed to outside light. This light exposure could have activated the screen and therefore cause more background than originally present in the black box.

For extracted, DOTA-labelled ^{68}Ga, the solution contained BPHA contamination in the DOTA-labelling process. When the nuclides stay chelated with BPHA contamination they are unavailable for DOTA-labelling, and therefore the labelling efficiency would decrease. The iTLC strips (3A) and (3B) in Figure 4.1 were made from two different back extraction solutions. The UV-Vis measurements of these extraction solutions were presented in Section 4.2. It was discovered that the solution for iTLC strip (3A)

contained a higher BPHA contamination, while the solution for iTLC strip (3B) had almost no contamination.
When the UV-Vis is compared to the phosphor image, it was seen that although the average labelling efficiency was 70.8670%, the uncertainty was $\pm$ 41.6798%. This high uncertainty comes from the differences in labelling efficiency per labelling batch. A high BPHA concentration measured in extraction solution 1 caused an average labelling efficiency of 11.9376%. Keeping in mind the influence of the reference strip on the 1A iTLC strip, this labelling efficiency was even lower when 1A was excluded from calculations. In extraction solution 2 a low BPHA contamination was measured, and the labelling efficiency reached 101.438%, passing the 100% due to negative intensities after the background was subtracted. It is suggested that high BPHA concentration in extraction solutions causes low labelling efficiency of ^{68}Ga to DOTA. However, the contamination of BPHA in the solutions used for DOTA-labelling was merely addressed as being present, and not measured quantitatively. Due to dilution the contamination concentrations in the experiments are not representative for the extraction solutions used in cyclotron production of ^{68}Ga.

5.2. Washing BPHA contamination from the extraction solutions

In Figure 5.1.a, graph (b) shows the characteristic absorption spectrum of 0.1mM BPHA + 20mM $Ga(ClO_4)_3$ [36]. The complex has an absorption peak at 270nm, a decrease around 230nm and increases below 240nm. In Figure 5.1 the reference spectrum is put next to the UV-Vis spectrum of the extraction solution 1 from Chapter 4.3 for comparison. In the reference spectrum the two characteristic absorption peaks lie between 0.4 and 0.8 on the y-axis for the BPHA complex with ^{68}Ga. There was no ^{68}Ga present during the washing process, so the graph for extraction solution 1 should not show any BPHA complexes. Although the extraction solution does show two absorption peaks they are not exaggerated enough to be assigned as complex peaks and can be assigned as characteristic BPHA peaks.

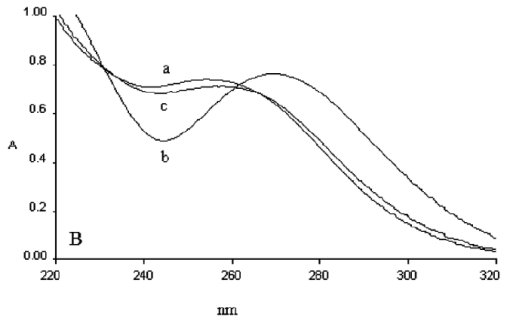

(a) Graph (b) shows the characteristic absorption spectrum of 0.1mM BPHA + 20mM $Ga(ClO_4)_3$ [36]

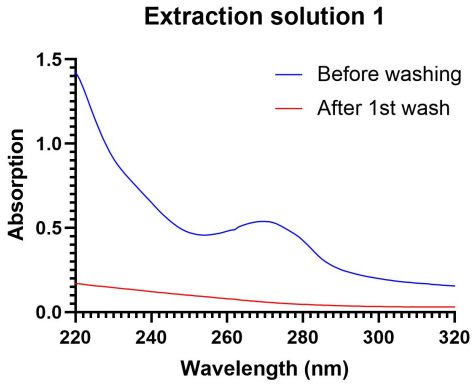

(b) UV-Vis spectrum of extraction solution 1 before and after washing with chloroform. Reference 0.1M HCl.

Figure 5.1: Comparison of the characteristic absorption spectrum for BPHA and the measured UV-Vis absorption spectrum for extraction solution 1 before and after washing.

It can be seen from Figure 5.1.b that the starting BPHA contamination concentration decreased after one wash. Figure 5.2, graph (a), shows the UV-Vis absorption spectrum of pure distilled water [20]. Comparing this absorption spectrum to Figure 5.1.b, the remaining absorption after one wash could be assigned to the solvent. This suggests that chloroform washing is a successful method to remove BPHA contamination from the extraction solutions.

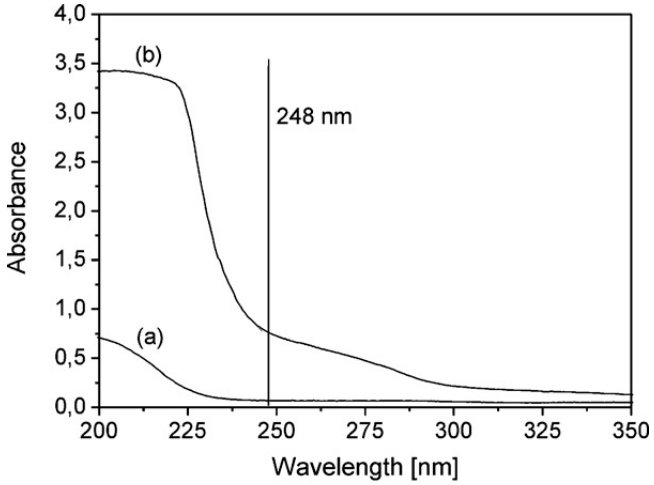

Figure 5.2: UV-Vis absorption spectrum of (a) pure distilled water [20].

In Figure 4.3, Chapter 4.2, the red line showed the BPHA contamination in the extraction solution used for the labelling batch 2. In the phosphor imaging process this solution was deemed to have a low enough BPHA concentration to result in a labelling efficiency of 101.438%. For extraction solution used in batch 3, the green line in Figure 4.3, also showed presence of BPHA contamination. This solution resulted in 99.2265% labelling efficiency. These results can set the bar for BPHA contamination for extraction solutions used in DOTA-labelling. The washed extraction solutions from Figure 4.4, 4.5 and 4.6 all showed BPHA contamination lower than extraction solution 2 in Figure 4.3. These washed extraction solutions should have a contamination level low enough to ensure up to 100% labelling efficiency.

6

Conclusion

In this report two research questions were answered:
1. Does BPHA contamination influence the labelling efficiency of ^{68}Ga radionuclides to the DOTA labelling link?
2. Can the BPHA contamination be removed from the final extraction solution, when ^{68}Ga is produced from enriched ^{68}Zn target solutions?

For this research, ^{68}Ga solutions were prepared with and without BPHA contamination.
It was found that for ^{68}Ga solutions without BPHA contamination the average labelling efficiency reached 102.3% $\pm$ 2.5%. The 100% was surpassed as some intensities in the ImageQuant TL Analysis turned negative as they were corrected for background. In the Wallac gamma counter the average labelling efficiency was calculated to be 99.58% $\pm$ 0.07%.
For ^{68}Ga solutions with BPHA, the average labelling efficiency became 70.8670% $\pm$ 41.6798%. The extraction solutions used for labelling were measured in UV-Vis absorption. The absorption spectra showed major differences in BPHA contamination concentration between the extraction solutions, causing the high uncertainty in the average labelling efficiency. The extraction solution with the lowest BPHA contamination was found to have a labelling efficiency of 101.438%. Its UV-Vis absorption spectrum could set the maximum for BPHA contamination in future extraction solutions. Keeping the contamination below this level would ensure high efficiency labelling.

Comparing the two average labelling efficiencies, it can be concluded that BPHA negatively affects the labelling of ^{68}Ga to DOTA. It can also be concluded that the effect of BPHA contamination depends on its concentration in the labelling solution.

In washing experiments the extraction solutions containing BPHA contamination were washed with chloroform. In UV-Vis absorbance the spectra showed a decrease in BPHA contamination after one wash. As the remaining absorbance can be assigned to the solvent, it is concluded that chloroform washing is a highly effective way of removing the BPHA contamination.

7

Recommendations

For future phosphor imaging of iTLC strips, the strips should be placed further apart from each other. This might significantly increase the measurement time, but ensures that the strips do not influence each other during exposure. This way the labelling efficiency can be calculated more reliably.

The contamination of BPHA in the solutions used for DOTA-labelling was merely addressed as being present, and not measured quantitatively. Due to dilution the contamination concentrations in the experiments are not representative for the extraction solutions used in cyclotron production of ^{68}Ga. Further research can include determining the concentrations of BPHA in labelling solutions, and the effect of different concentrations on DOTA-labelling. It could be decided whether this effect follows a trend linear to the contamination concentration. Also, it can be investigated whether the effect holds for a threshold contamination concentration. If so, the back extraction solutions should be washed below this threshold to ensure successful labelling.

The washed solutions in this research were not used for further labelling processes. However, the UV-Vis spectra of the BPHA contamination after one wash showed promising removal of the contamination. Adding the DOTA-labelling process after washing the back extraction solutions could further prove successful washing, as this would be reflected in a high labelling efficiency.

[18]

References

[1] International Atomic Energy Agency (IAEA). *Gallium-68 Cyclotron Production*. IAEA TECDOC series, ISSN 1011–4289 ; no. 1863. IAEA, 2019.

[2] National Health Service (NHS). *PET Scan*. Mar. 2021. URL: https://www.nhs.uk/conditions/pet-scan/.

[3] Agilent. *Chromatography Papers: iTLC-SG*. Retreived June 28, 2022. URL: https://www.agilent.com/en/product/thin-layer-chromatography/chromatography-papers/itlc-sg.

[4] Muhammad Sajid Akash and Kanwal Rehman. *Ultraviolet-visible (UV-vis) spectroscopy*. Spring Singapore, Dec. 2019, pp. 29–56. DOI: 10.1007/978-981-15-1547-7_3.

[5] Sigma Aldrich. *Thin Layer Chromatography (TLC)*. Retreived June 28, 2022. URL: https://www.sigmaaldrich.com/SE/en/products/analytical-chemistry/analytical-chromatography/tlc-plates-and-adsorbants.

[6] F. Alves et al. "Cyclotron production of Ga-68 for human use from liquid targets: From theory to practice". In: *AIP Conference Proceedings* 1845.1 (May 2017). DOI: 10.1063/1.4983532.

[7] Dipa Aryal. *Chelating agent: Definition, examples, and applications*. May 2022. URL: https://chemistnotes.com/inorganic/chelating-agent/.

[8] Giuliano Bandoli et al. "Mononuclear six-coordinated Ga(III) complexes: A comprehensive survey". In: *Coordination Chemistry Reviews* 253.1 (2009), pp. 56–77. ISSN: 0010-8545. DOI: https://doi.org/10.1016/j.ccr.2007.12.001. URL: https://www.sciencedirect.com/science/article/pii/S0010854507002949.

[9] Zsolt Baranyai, Gyula Tircsó, and Frank Rösch. "The use of the macrocyclic chelator DOTA in radiochemical separations". In: *European Journal of Inorganic Chemistry* 2020.1 (Oct. 2019), pp. 36–56. DOI: 10.1002/ejic.201900706.

[10] Marie-Martine Bé et al. "Table of Radionuclides: Comments on Evaluations". In: *Monographie BIPM-5* 1-7 (2008).

[11] CBS. *Deaths; underlying cause of death (shortlist), sex, age*. June 2022. URL: https://www.cbs.nl/en-gb/figures/detail/7052eng.

[12] Gregory Choppin et al. *Radiochemistry and nuclear chemistry*. 4th ed. Elsevier, 2013.

[13] E. Creutz and Bernard L. Cohen. "Cyclotrons and Synchrocyclotrons". In: *Nuclear Instrumentation I / Instrumentelle Hilfsmittel der Kernphysik I*. 1st ed. Springer Berling, 1959, pp. 105–169.

[14] Janet F. Eary. "PET imaging for treatment response in cancer". In: *PET Clinics* 3.1 (Jan. 2008), pp. 101–109. DOI: 10.1016/j.cpet.2008.10.001.

[15] J.W. Engle et al. "Very high specific activity 66/68Ga from zinc targets for PET". In: *Applied Radiation and Isotopes* 70.8 (Aug. 2012), pp. 1792–1796. DOI: 10.1016/j.apradiso.2012.03.030.

[16] Ljudmila Fele Žilnik and Blaž Likozar. "Back-extraction process operation and modeling through thermodynamic equilibrium solubility of valeric acid in aqueous and organic phase mixtures". In: *Separation and Purification Technology* 222 (Sept. 2019), pp. 125–135. DOI: 10.1016/j.seppur.2019.04.033.

[17] Maram Ghadban. *Acetonitrile: Structure and Formula*. Feb. 2021. URL: https://study.com/learn/lesson/acetonitrile.html.

[18] Siemens Healthcare GmbH. *PET/CT scanners*. 2022. URL: https://www.siemens-healthineers.com/molecular-imaging/pet-ct.

[19] Michal Grzmil et al. "An overview of targeted radiotherapy". In: *Radiopharmaceutical Chemistry* (Apr. 2019), pp. 85–100. DOI: 10.1007/978-3-319-98947-1_5.

[20] Enikö György et al. “Processing and immobilization of chondroitin-4-sulphate by UV laser radiation”. In: *Colloids and Surfaces B: Biointerfaces* 104 (Jan. 2013), p. 169.

[21] François-Xavier Hanin et al. “Tumor uptake of 68ga-DOTA-Tyr3-octreotate: Animal pet studies of tumor flow and acute somatostatin receptor modulation in the CA20948 RAT model”. In: *Nuclear Medicine and Biology* 37.2 (Feb. 2010), pp. 157–165. DOI: 10.1016/j.nucmedbio.2009.09.006.

[22] Ute Hennrich and Martina Benešová. “[68ga]ga-DOTA-TOC: The first FDA-approved 68ga-radiopharmaceutical for PET imaging”. In: *Pharmaceuticals* 13.3 (Mar. 2020), p. 38. DOI: 10.3390/ph13030038.

[23] Orit Jacobson, Dale O. Kiesewetter, and Xiaoyuan Chen. “Fluorine-18 radiochemistry, labeling strategies and synthetic routes”. In: *Bioconjugate Chemistry* 26.1 (Jan. 2015), pp. 1–18. DOI: 10.1021/bc500475e.

[24] Amir Reza Jalilian. “An overview on Ga-68 radiopharmaceuticals for positron emission tomography applications”. In: *Iranian Journal of Nuclear Medicine* 24.1 (Jan. 2016), pp. 1–10.

[25] Krzysztof Kilian. “68Ga-dota and analogs: Current status and future perspectives”. In: *Reports of Practical Oncology amp; Radiotherapy* 19 (May 2014). DOI: 10.1016/j.rpor.2014.04.016.

[26] Vojtěch Kubíček et al. “Gallium(III) complexes of DOTA and dota−monoamide: Kinetic and thermodynamic studies”. In: *Inorganic Chemistry* 49.23 (2010), pp. 10960–10969. DOI: 10.1021/ic101378s.

[27] Krishan Kumar. “The current status of the production and supply of gallium-68”. In: *Cancer Biotherapy and Radiopharmaceuticals* 35.3 (Apr. 2020), pp. 163–166. DOI: 10.1089/cbr.2019.3301.

[28] P.B. Kyle. “Toxicology: GCMS”. In: *Mass Spectrometry for the Clinical Laboratory* (2017). Ed. by Hari Nair and WilliamEditors Clarke, pp. 131–163. DOI: 10.1016/b978-0-12-800871-3.00007-9.

[29] Mai Lin et al. “Long-term evaluation of Tio2-based 68ge/68GA generators and optimized automation of [68GA]DOTATOC radiosynthesis”. In: *Applied Radiation and Isotopes* 70.10 (Oct. 2012), pp. 2539–2544. DOI: 10.1016/j.apradiso.2012.05.009.

[30] Fei Liu et al. “68Ga/177Lu-labeled DOTA-TATE shows similar imaging and biodistribution in neuroendocrine tumor model”. In: *Tumor Biology* 39.6 (June 2017), pp. 1–9. DOI: 10.1177/1010428317705519.

[31] M. Stanley Livingston. “The Cyclotron. I”. In: *Journal of Applied Physics* 15 (1944), p. 2. DOI: 10.1063/1.1707364.

[32] S. J. Lyle and A. D. Shendrikar. “A separation scheme for gallium, indium, thallium, germanium, tin and lead by solvent extraction with N-benzoyl-N-phenylhydroxylamine”. In: *Analytica Chimica Acta* 32 (1965), pp. 575–582. DOI: 10.1016/s0003-2670(01)84927-8.

[33] Minhui Ma and Frederick F. Cantwell. “Solvent microextraction with simultaneous back-extraction for sample cleanup and preconcentration: preconcentration into a single Microdrop”. In: *Analytical Chemistry* 71.2 (1999), pp. 388–393. DOI: 10.1021/ac9805899.

[34] Roberta Santos Marinho, Julio Carlos Afonso, and José Waldemar da Cunha. “Recovery of platinum from spent catalysts by liquid–liquid extraction in Chloride Medium”. In: *Journal of Hazardous Materials* 179.1-3 (Mar. 2010), pp. 488–494. DOI: 10.1016/j.jhazmat.2010.03.029.

[35] Priscila G Mazzola et al. “Liquid–liquid extraction of biomolecules: An overview and update of the main techniques”. In: *Journal of Chemical Technology amp; Biotechnology* 83.2 (2008), pp. 143–157. DOI: 10.1002/jctb.1794.

[36] Lauretta Morroni et al. “Kinetics and equilibria of the interactions of hydroxamic acids with gallium(iii) and indium(iii)”. In: *Inorganic Chemistry* 43.9 (Sept. 2004), pp. 3005–3012. DOI: 10.1021/ic034781r.

[37] Eckart Müller et al. “Liquid-liquid extraction”. In: *Ullmann’s Encyclopedia of Industrial Chemistry* (2008). DOI: 10.1002/14356007.b03_06.pub2.

[38] Mukesh K. Pandey et al. “Cyclotron production of 68Ga via the 68Zn(p,n)68Ga reaction in aqueous solution”. In: *American Journal of Nuclear Medicine and Molecular Imaging* 4.4 (June 2014), pp. 303–310.

[39] Donald L. Pavia et al. “Ultraviolet Spectroscopy”. In: *Introduction to spectroscopy*. Fifth. Cengage Learning, 2015, pp. 577–613.

[40] PubChem. *Chloroform*. URL: https://pubchem.ncbi.nlm.nih.gov/compound/Chloroform#section=Boiling-Point.

[41] PubChem. *PubChem Compound Summary for CID 121841, Tetraxetan*. 2022. URL: https://pubchem.ncbi.nlm.nih.gov/compound/Tetraxetan#section=Structures.

[42] V. Radchenko et al. “Separation of 90Nb from zirconium target for application in immuno-PET”. In: *Radiochimica Acta* 102.5 (2014), pp. 433–442. DOI: 10.1515/ract-2013-2156.

[43] Michael J. Raphael et al. “Principles of diagnosis and management of neuroendocrine tumours”. In: *Canadian Medical Association Journal* 189.10 (Mar. 2017), E398–E404. DOI: 10.1503/cmaj.160771.

[44] Jean Claude Reubi et al. “Affinity Profiles for human somatostatin receptor subtypes SST1-SST5 of somatostatin radiotracers selected for scintigraphic and radiotherapeutic use”. In: *European Journal of Nuclear Medicine and Molecular Imaging* 27.3 (2000), pp. 273–282. DOI: 10.1007/s002590050034.

[45] Fellipy S. Rocha et al. “Experimental methods in chemical engineering: Ultraviolet visible spectroscopy-UV-vis”. In: *The Canadian Journal of Chemical Engineering* 96.12 (Dec. 2018), pp. 2512–2517. DOI: 10.1002/cjce.23344.

[46] Isotope Rosatom. *Gallium-68 Generator (Ge-68/Ga-68)*. URL: http://www.isotop.ru/en/production/medical/427/446/.

[47] F. Rösch. “Past, present and future of 68Ge/68Ga generators”. In: *Applied Radiation and Isotopes* 76 (2013), pp. 24–30. DOI: 10.1016/j.apradiso.2012.10.012.

[48] J A Rowlands. “The physics of computed radiography”. In: *Physics in Medicine and Biology* 47.23 (Dec. 2002). DOI: 10.1088/0031-9155/47/23/201.

[49] Vittoria Rufini, Maria Lucia Calcagni, and Richard P. Baum. “Imaging of neuroendocrine tumors”. In: *Seminars in Nuclear Medicine* 36.3 (July 2006), pp. 228–247. DOI: 10.1053/j.semnuclmed.2006.03.007.

[50] Mahdi Sadeghi et al. “Cyclotron production of 68Ga via proton-induced reaction on 68Zn target”. In: *Nukleonika* 54.1 (2009), pp. 25–28.

[51] Gopal B. Saha. *Basics of Pet Imaging: Physics, Chemistry, and regulations*. Third. Springer, 2016.

[52] Dhananjay Bhaskar Sarode et al. “Separation and removal of cu2+, fe2+, and fe3+from environmental waste samples by N-benzoyl-n-phenylhydroxylamine”. In: *Environmental Technology* 36.4 (2014), pp. 521–528. DOI: 10.1080/09593330.2014.979250.

[53] University of Saskatchewan and Fedoruk Centre. *What is a cyclotron?* URL: https://fedorukcentre.ca/resources/what-is-a-cyclotron.php.

[54] Rajnish Sharma et al. “A comparison study of11C-methionine and18F-fluorodeoxyglucose positron emission tomography-computed tomography scans in evaluation of patients with recurrent brain tumors”. In: *Indian Journal of Nuclear Medicine* 31.2 (Apr. 2016), pp. 93–102. DOI: 10.4103/0972-3919.178254.

[55] Sigma-Aldrich. 2022. URL: https://www.sigmaaldrich.com/SE/en/search/chloroform?focus=products&page=1&perpage=30&sort=relevance&term=chloroform&type=product_name.

[56] Sigma-Aldrich. *N-benzoyl-N-phenylhydroxylamine (BPHA)*. 2022. URL: https://www.sigmaaldrich.com/SE/en/product/aldrich/274852.

[57] Courtney Slough et al. “Clinical positron emission tomography (PET) neuroimaging: Advantages and limitations as a diagnostic tool”. In: *The Journal of Neuropsychiatry and Clinical Neurosciences* 28.2 (Apr. 2016), A4–71. DOI: 10.1176/appi.neuropsych.16030044.

[58] John C. Stendahl and Albert J. Sinusas. “11C-acetate PET: A powerful tool to analyze metabolic and functional changes in the heart related to alcohol consumption”. In: *Journal of Nuclear Cardiology* 29.1 (July 2020), pp. 289–292. DOI: 10.1007/s12350-020-02268-0.

[59] Hyuna Sung et al. “Global cancer statistics 2020: Globocan estimates of incidence and mortality worldwide for 36 cancers in 185 countries”. In: *CA: A Cancer Journal for Clinicians* 71.3 (Feb. 2021), pp. 209–249. DOI: 10.3322/caac.21660.

[60] Nathalie Testart Dardel et al. “Clinical applications of pet using C-11/F-18-choline in brain tumours: A systematic review”. In: *Clinical and Translational Imaging* 5 (July 2016), pp. 101–119. DOI: 10.1007/s40336-016-0200-0.

[61] Roy S. Tilbury and John S. Laughlin. “Cyclotron production of radioactive isotopes for medical use”. In: *Seminars in Nuclear Medicine* 4.3 (1974), pp. 245–255. DOI: 10.1016/s0001-2998(74)80012-7.

[62] S. Trapp. *Ongoing research at Reactor Instituut Delft, Applied Radiation Isotopes research group*.

[63] Juan José Vaquero and Paul Kinahan. “Positron emission tomography: Current challenges and opportunities for technological advances in clinical and Preclinical Imaging Systems”. In: *Annual Review of Biomedical Engineering* 17.1 (2015), pp. 385–414. DOI: 10.1146/annurev-bioeng-071114-040723.

[64] Irina Velikyan. “68ga-based radiopharmaceuticals: Production and application relationship”. In: *Molecules* 20.7 (July 2015), pp. 12913–12943. DOI: 10.3390/molecules200712913.

[65] Thaddeus J. Wadas et al. “Coordinating radiometals of copper, gallium, indium, yttrium, and zirconium for PET and SPECT imaging of disease”. In: *Chemical Reviews* 110.5 (Sept. 2010), pp. 2858–2902. DOI: 10.1021/cr900325h.

[66] Wolfgang A. Weber and Hinrich Wieder. “Monitoring chemotherapy and radiotherapy of solid tumors”. In: *European Journal of Nuclear Medicine and Molecular Imaging* 33 (May 2006), pp. 27–37. DOI: 10.1007/s00259-006-0133-3.

[67] Damian Wild et al. “DOTA-NOC, a high-affinity ligand of somatostatin receptor subtypes 2, 3 and 5 for labelling with various radiometals”. In: *European Journal of Nuclear Medicine and Molecular Imaging* 30.10 (Aug. 2003), pp. 1338–1347. DOI: 10.1007/s00259-003-1255-5.

[68] W.M. van Wyngaardt et al. “Development of the Australian standard for germanium-68 by two liquid scintillation counting methods”. In: *Applied Radiation and Isotopes* 134 (Apr. 2018), pp. 79–84. DOI: 10.1016/j.apradiso.2017.10.005.

[69] Run Yu. “Neuroendocrine tumors”. In: *Reference Module in Biomedical Sciences* (2018). DOI: 10.1016/b978-0-12-801238-3.00012-x.

A

Phosphor imaging

In Appendix A the complete phosphor images as discussed in Chapter 4 are included for the three different ^{68}Ga solutions: Extracted and unlabelled (1) in A.3, eluted and labelled (2) in A.2, and extracted and labelled (3) in A.3. On the images, the far left strip is the reference strip with eluted ^{68}Ga activity applied 3 cm from the top and 3 cm from the bottom of the iTLC strip. Three batches were made for every ^{68}Ga solution, and were named batch 1, 2 and 3. For every batch, three iTLC strips were made, named A, B and C, totalling 9 iTLC strips per ^{68}Ga solution in the phosphor imager. The green borders indicate the selected area in the ImageQuant TL Toolbox, used in labelling efficiency calculations in section 4.1.

A.1. Extracted, unlabelled ^{68}Ga solution

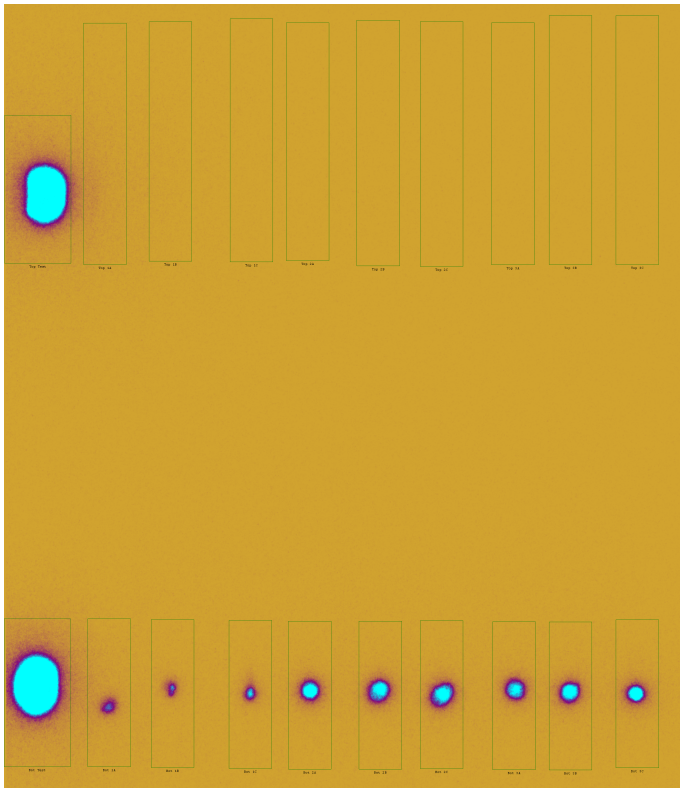

Figure A.1: Phosphor imaging of unlabelled ^{68}Ga extracted from the target solution on iTLC strips. Left strip serves as marker strip, then from left to right three iTLC strips for batch 1, 2 and 3 respectively.

A.2. Eluted, DOTA-labelled ^{68}Ga solution

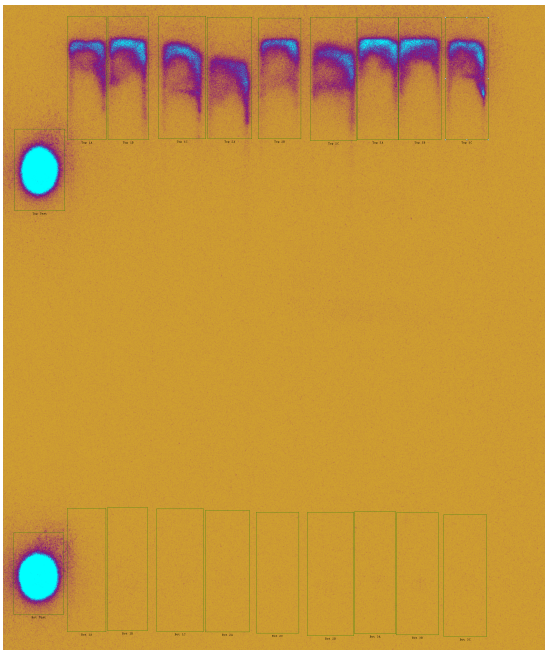

Figure A.2: Phosphor imaging of DOTA-labelled ^{68}Ga eluted from the generator on iTLC strips. Left strip serves as marker strip, then from left to right three iTLC strips for batch 1, 2 and 3 respectively.

A.3. Extracted, DOTA-labelled ^{68}Ga solution

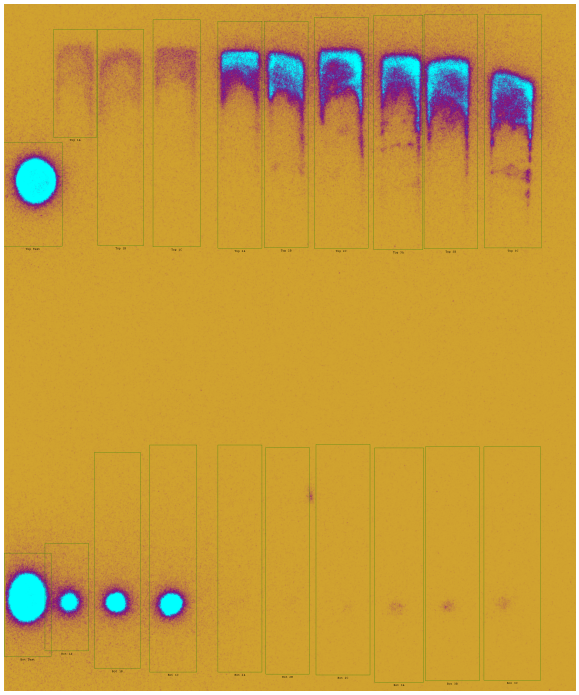

Figure A.3: Phosphor imaging of DOTA-labelled ^{68}Ga extracted from the target solution on iTLC strips. Left strip serves as marker strip, then from left to right three iTLC strips for batch 1, 2 and 3 respectively.

B

Raw data

Appendix B.1 provides the raw data of this research. The Wallac measurements were taken after the labelling and iTLC process for eluted, DOTA-labelled ^{68}Ga solution. In Section B.2 the raw data for the ImageQuant TL Analysis Toolbox is included, which was used in calculations of the labelling efficiency. For the ImageQuant, the units were in arbitrary units (a.u.).
Three batches were made for every ^{68}Ga solution, and were named batch 1, 2 and 3. For every batch, three iTLC strips were made, named A, B and C, totalling 9 iTLC strips per ^{68}Ga solution in the phosphor imager.

B.1. Wallac gamma counter

The iTLC strips 1A, 2A and 3A from the eluted, labelled ^{68}Ga solution were measured for their activity at the top, 'Top' and bottom, 'Bot', of the strip. The strips were cut into pieces of 4 cm. The raw data is presented in table B.1. The measurement time in the Wallac gamma counter was 2 minutes. The counts per minute (cpm) was corrected for background. The activity was calculated using the given efficiency factor of 0.0321 Bq/cpm of the Wallac gamma counter. In section 4.1 the data is used in labelling efficiency calculation, using Equation 2.1 from section 2.3.1.

Table B.1: Raw data for the Wallac gamma counter for the 1A, 2A and 3A iTLC strips from eluted, DOTA-labelled ^{68}Ga solution.

iTLC	Measurement Time (s)	Ga-68 Counts	Ga-68 CPM	Corrected CPM for background	Activity (Bq)
Top 1A	120.05	16882.98	8445.43	8416.94	270
Bot 1A	120.04	144	71.97	43.48	1.40
Top 2A	120.03	16013.2	8011.36	7982.87	256
Bot 2A	120.05	122.55	61.25	32.76	1.05
Top 3A	120.05	15900.57	7953.79	7925.3	254
Bot 3A	120.05	110.78	55.37	26.88	0.863

B.2. ImageQuant TL Analysis Toolbox

In this section the raw data of the ImageQuant TL Analysis Toolbox on the phosphor imaging figures is presented as discussed in chapter 4. Data for the extracted and unlabelled ^{68}Ga solution, eluted and labelled ^{68}Ga solution and exracted and labelled ^{68}Ga solution can be found in Table B.2, B.3 and B.4 respectively. All values in the table are in arbitrary units (a.u.). In the toolbox, areas on the iTLC were chosen, which are depicted with green borders in Appendix A, and called 'Area' in the tables. The average intensity was measured, and by multiplying this with the area, the total intensity was obtained. The total intensity was corrected for the background.

Table B.2: ImageQuant TL Analysis of bottom 'Bot' and top 'Top' parts of the iTLC strips from unlabelled, extracted ^{68}Ga seen in Figure A.1.

Selection	Background	Average Intensity	Area	Total intensity	Corrected total intensity
Bot 1A	1321542	25.87	88640	2293117	971575
Bot 1B	586932.3	15.81	88640	1401398	814466
Bot 1C	534923.7	19.26	88640	1707206	1172283
Top 1A	1808741	12.64	144640	1828250	19509
Top 1B	591275.5	4.18	143360	599245	7969
Top 1C	250796.7	1.85	145600	269360	18563
Bot 2A	693832.5	55.08	88640	4882291	4188458.7
Bot 2B	743475.3	52.94	88640	4692602	3949126.3
Bot 2C	846684.1	57.45	88640	5092368	4245683.9
Top 2A	187536	1.31	142400	186544	-992.03
Top 2B	157816.9	1.08	147200	158976	1159.06
Top 2C	144839.8	0.91	146560	133369.6	-11470.17
Bot 3A	707725.2	42.7	88640	3784928	3077202.8
Bot 3B	717068.7	49.44	88640	4382362	3665293
Bot 3C	677636.9	50.21	88640	4450614	3772977.5
Top 3A	128408.2	0.89	144960	129014.4	606.22
Top 3B	133284.1	0.89	149120	132716.8	-567.25
Top 3C	131066.7	0.8	149120	119296	-11770.68

Table B.3: ImageQuant TL Analysis of bottom 'Bot' and top 'Top' parts of the iTLC strips from labelled, eluted ^{68}Ga seen in Figure A.2

Selection	Background	Average Intensity	Area	Total intensity	Corrected total intensity
Bot 1A	702868.3	6.28	92480	580774.4	-122093.9
Bot 1B	344278.5	3.52	96476	339595.5	-4682.95
Bot 1C	348576.7	3.09	112320	347068.8	-1507.9
Top 1A	1316337	23.25	92480	2150160	833823.38
Top 1B	1339075	27.02	96476	2606782	1267706.4
Top 1C	1193308	25.85	112320	2903472	1710164
Bot 2A	293372.2	2.88	103984	299473.9	6101.68
Bot 2B	305006.7	2.66	110976	295196.2	-9810.53
Bot 2C	273573.2	2.67	100016	267042.7	-6530.44
Top 2A	1220615	23.23	103984	2415548	1194933.2
Top 2B	1066457	22.45	100016	2245359	1178902.5
Top 2C	1440156	26.72	110976	2965279	1525122.5
Bot 3A	281462.4	2.68	97916	262414.9	-19047.53
Bot 3B	270778.5	2.75	100068	275187	4408.49
Bot 3C	290515.7	2.77	101144	280168.9	-10346.82
Top 3A	1814310	27.47	97916	2689753	875442.27
Top 3B	1619445	25.39	100068	2540727	921281.37
Top 3C	1050808	25.51	101144	2580183	1529375.2

Table B.4: ImageQuant TL Analysis of bottom 'Bot' and top 'Top' parts of the iTLC strips from labelled, extracted ^{68}Ga seen in Figure A.3

Selection	Background	Average Intensity	Area	Total intensity	Corrected total intensity
Bot 1A	2939243.01	58.85	91008	5355821	2416577.8
Bot 1B	1201335.25	29.9	192304	5749890	4548554.4
Bot 1C	1011746.52	31.31	208000	6512480	5500733.5
Top 1A	549104.82	10.79	91008	981976.3	432871.5
Top 1B	955400.45	7.52	192304	1446126	490725.63
Top 1C	1011116.65	8.09	208000	1682720	671603.35
Bot 2A	426061.44	1.92	194000	372480	-53581.44
Bot 2B	345283.11	1.27	191616	243352.3	-101930.79
Bot 2C	219232.15	0.88	241808	212791	-6441.11
Top 2A	1983526.99	27.08	194000	5253520	3269993
Top 2B	2420552.86	34.19	191616	6551351	4130798.2
Top 2C	2791407.71	34.26	241808	8284342	5492934.4
Bot 3A	188527.52	0.91	222912	202849.9	14322.4
Bot 3B	142370.57	0.83	243552	202148.2	59777.59
Bot 3C	149742.14	0.81	257000	208170	58427.86
Top 3A	3321563.15	35.31	222912	7871023	4549459.6
Top 3B	3565136.05	37.69	243552	9179475	5614338.8
Top 3C	2182397.5	32.12	257000	8254840	6072442.5